ELSEVIER

International Journal of Adhesion & Adhesives 27 (2007) 611–620

International Journal of Adhesion & Adhesives

www.elsevier.com/locate/ijadhadh

An original epoxy-stamp on glass-disc specimen exhibiting stable debonding for identifying adhesive properties between glass and epoxy

A. Sekulic*, A. Curnier

Laboratory of Applied Mechanics and Reliability Analysis, Ecole Polytechnique Fédérale de Lausanne, CH-1015, Switzerland

Accepted 13 April 2006
Available online 22 December 2006

Abstract

An original axisymmetric specimen composed of a concave epoxy-stamp bonded on a glass-disc, which exhibits stable decohesion under traction, is proposed for identifying the adhesive properties, namely the adhesion surface energy, the adhesion peak stress and the decohesion rupture gap between glass and epoxy. Debonding stability is obtained by combining two stabilizing effects of the epoxy-stamp geometry: axisymmetry and concavity. This stamp design is believed to be an important discovery since stable crack propagation is the exception rather than the rule in fracture mechanics. The increasing graph of the traction force vs. the specimen elongation enables to measure the adhesion surface energy upon unloading, calculate the adhesion peak stress and deduce the decohesion rupture gap. Preliminary experiments confirm the stability of the debonding process and show excellent reproducibility.

Keywords: Epoxy/epoxides; Glass; Fracture; Adhesion

1. Introduction

In Contact Mechanics and Tribology, *adhesion* is the conservative reversible normal relation (contiguity) and attractive interaction (tension) at the interface between two materials in contact. ''Deadhesion'' is the loss of adhesion, i.e. the dissipative irreversible normal gap increase and tension decrease at the interface between two debonding materials.

Adhesion at an interface between two materials is analogous to rigid or elastic tension–dilatation *cohesion* in the bulk of one material; ''Deadhesion'' at an interface is analogous to rigid or elastic and plastic damage or decohesion in the bulk. This is why ''Deadhesion'' will be called *decohesion* in the sequel, to conform with common usage.

Adherence and *decoherence* are the tangential components of adhesion and decohesion, respectively. Bonding is the composition of normal adhesion and tangential adherence. Debonding that of decohesion and decoherence.

In Fracture Mechanics and Rheology, debonding is usually interpreted as a crack propagating along the material pair interface at the microscale and as damage at the macroscale. Normal adhesion–decohesion and tangential adherence–decoherence at an existing contact interface are very similar to normal (mode I) cohesion–decohesion and tangential (modes II and III) coherence–decoherence at a crack front in the bulk of a material.

Adhesion and adherence phenomena are not fully understood yet and both their formulation and identification can still be improved. Adhesion and adherence play an important role in several technologies: adhesive (Scotch) tapes, glues, machine part assembly, composite materials, tyres, wipers, biomechanics (biomaterials, living tissues), ...

This study is motivated by the fibre–matrix debonding which occurs in glass fibre reinforced epoxy matrix composites and decreases their strength. In this article, we focus our attention on the identification of the adhesive properties between glass and epoxy.

The basic *adhesive property*, entering a normal adhesion–decohesion law relating the normal tensile stress p_n to the normal gap g_n at an interface, is the *surface energy of*

*Corresponding author. Tel.: +41 21 693 3871; fax: +41 21 693 7340.
E-mail address: aleksandar.sekulic@epfl.ch (A. Sekulic).

0143-7496/$ - see front matter © 2007 Elsevier Ltd. All rights reserved.
doi:10.1016/j.ijadhadh.2006.04.004

adhesion (per unit area) ω (of Dupré). It represents the local work dissipated during the decohesion process (i.e. at the particle pair or continuum elementary area microscale). In several contact mechanics models of adhesion–decohesion, the surface energy ω is equal to the product of two other basic adhesive properties, namely the *adhesion peak stress* π_n and the *decohesion rupture gap* γ_n, or rather a fraction of it (e.g. one half),

$$\omega = \tfrac{1}{2}\pi_n\gamma_n. \tag{1}$$

These adhesive properties are difficult to measure accurately because the decohesion process is often unstable. Locally (i.e. at the particle pair microscale), decohesion always is an *unstable* phenomenon, meaning that the normal tensile stress p_n is an (abruptly) decreasing function of the normal gap g_n. Globally (i.e. at the specimen macroscale), decohesion can become *stable*, meaning that the normal traction force $f = \overline{p}_n$ applied to the specimen remains an increasing function of its normal elongation $u = \overline{g}_n$, due to subtle geometrical effects. Stable global decohesion is the exception rather than the rule however [1].

The common experiments for studying normal *adhesion* are the *membrane peeling* experiment [2,3] and the *punch pulling* experiment (usually between elastomers and metals) (e.g. [4–6]).

Debonding is usually stable in the membrane peeling experiment, but not every material can be made into a membrane and bonded to the surface of another (only highly anisotropic, nearly inextensible, fibrous materials seem appropriate).

In the punch pulling experiment, convex punches with various profiles: flat, spherical, conical ... are pressed into a half-space and then pulled away. The adhesion peak stress and the rupture gap (or interface energy) are then deduced from the critical pulling force necessary to separate the punch from the half-space, via a Hertzian analysis (e.g. [7]). Debonding is always unstable in this experiment [8], so that the adhesive properties cannot be accurately measured.

In this article, we present an original *axisymmetric specimen composed of an epoxy-stamp bonded on a glass-disc*, which exhibits a stable decohesion under traction and hereby permits an accurate identification of the adhesive properties. Debonding stability is obtained by combining two stabilizing effects of the epoxy-stamp geometry: axisymmetry and concavity, discovered by analogy with two observations in contact and fracture mechanics, respectively. Preliminary experiments confirm the stability of the debonding process and show excellent reproducibility. A preliminary identification procedure of the adhesive properties promises a good accuracy.

This article is divided in six sections besides the present introduction and a final conclusion: (1) theoretical background, (2) specimen design, (3) specimen fabrication, (4) experimental procedure, (5) preliminary results, and (6) identification of adhesive properties.

2. Theoretical background

A complete formulation of *contact mechanics* between deformable solids undergoing large transformations can be found in Curnier et al. [9]. Here, only a summary of the relevant kinematic and static elements is given within the simplifying hypothesis of small displacements implying *small gaps* and *small slips*, along Talon and Curnier [10].

Consider two deformable solids which are about to (or already in) contact at the present time t (Fig. 1).

A particle is identified by its actual position vector $\boldsymbol{y}$. Within the hypothesis of small gaps and slips, the contact *gap vector* $\boldsymbol{g}$ at the present time, between a striker boundary particle at $\boldsymbol{y}$ and a target one at $\boldsymbol{y}'$ *initially in regards*, is simply defined by

$$\boldsymbol{g} = \boldsymbol{y} - \boldsymbol{y}'. \tag{2}$$

The gap velocity (rate) is equal to $\dot{\boldsymbol{g}} = \dot{\boldsymbol{y}} - \dot{\boldsymbol{y}}'$ where $\dot{\boldsymbol{y}} = \partial\boldsymbol{y}/\partial t$.

Dually, the contact pressure or *stress vector* $\boldsymbol{p}$ is defined as the stress vector applied by the target on the striker, as it occurs in the action–reaction principle

$$\boldsymbol{p} = -\boldsymbol{p}'. \tag{3}$$

Classically, both the gap and stress vectors can be decomposed into normal and tangential components along and across the unit outward normal $\boldsymbol{n}$ to the target surface, as

$$\boldsymbol{g} = g_n\boldsymbol{n} + \boldsymbol{g}_t, \quad \boldsymbol{p} = p_n\boldsymbol{n} + \boldsymbol{p}_t, \tag{4}$$

where $g_n \equiv \boldsymbol{g}\cdot\boldsymbol{n}$ is the normal *gap* ($g_n > 0 \leftrightarrow$ separation, $g_n < 0 \leftrightarrow$ penetration), $p_n \equiv \boldsymbol{p}\cdot\boldsymbol{n}$ the normal *pressure* ($p_n > 0 \leftrightarrow$ tension, $p_n < 0 \leftrightarrow$ pressure), $\boldsymbol{g}_t$ the tangential *slip* ($\|\dot{\boldsymbol{g}}_t\| = 0 \leftrightarrow$ grip, $\|\dot{\boldsymbol{g}}_t\| \neq 0 \leftrightarrow$ slip) and $\boldsymbol{p}_t$ the tangential *shear*.

With these geometric and static definitions in mind, the *tribological laws* which are relevant to this study can be defined as follows:

- A law of unilateral *contact* relates the normal gap g_n to the normal pressure p_n; it models the strong repulsive force which prevents any two materials to interpenetrate.
- A law of dry *friction* relates the tangential slip rate $\dot{\boldsymbol{g}}_t$ (and perhaps the pressure p_n) to the tangential shear $\boldsymbol{p}_t$;

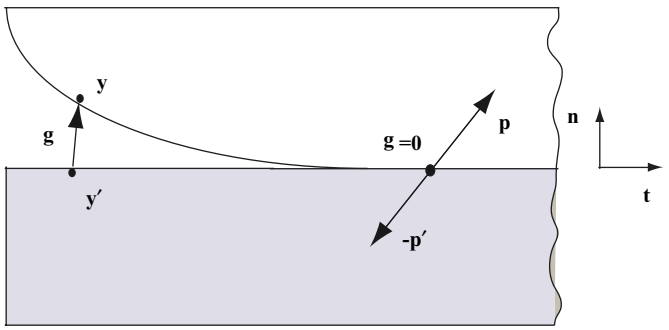

Fig. 1. Schematics of contact between two deformable solids.

it models the strong (apparently) attractive force opposed by two materials to their steady sliding (friction is attractive at the smooth interface scale but repulsive at the asperity scale).

- A law of *adhesion* (*–decohesion*) relates the normal gap g_n and its rate $\dot{g}_n$ to the normal tension p_n; it models the weak attractive force opposed by two materials to their separation.
- A law of *adherence* (*–decoherence*) relates the slip $\boldsymbol{g}_t$ and its rate $\dot{\boldsymbol{g}}_t$ to the shear $\boldsymbol{p}_t$; it models the weak (genuinely) attractive force opposed by two materials to their incipient sliding.

Unilateral contact is a conservative reversible process, whereas friction, decohesion and decoherence are dissipative irreversible processes.

The laws of unilateral contact and threshold friction have been coupled for a long time now, beginning with Mozynski [11] and Moreau [12] and pursuing with Fredrikson [13], Michalowski and Mroz [14], Curnier [15], Klarbring [16], Curnier and Alart [17]. Combining adhesion with unilateral contact is more recent [18–21]. Adding adherence to friction is quite recent [10,22–24]. All these laws (except that of friction proportional to pressure) can be derived from a nonsmooth energy potential and a nonsmooth dissipation potential using nonsmooth convex analysis.

The *graph of a simple contact-adhesion law* with instantaneous brittle (binary) decohesion (Curnier-Sekulic (in preparation)) is shown in Fig. 2.

Adhesion ceases when the tension stress reaches the *adhesion peak stress* π_n. Debonding occurs over the finite *decohesion rupture gap* γ_n. The work dissipated during decohesion (triangle area) is equal to the *adhesion surface energy* (per unit interface area) ω. Hence, the law involves only two different states: contact (-adhesion) and gap (-decohesion) and requires only two adhesive properties: π_n and γ_n (or ω).

This law is obviously unstable at its particle microscale (decreasing decohesion graph). The adhesive properties can be accurately measured in an experiment only if the debonding process is stable at its specimen macroscale [1].

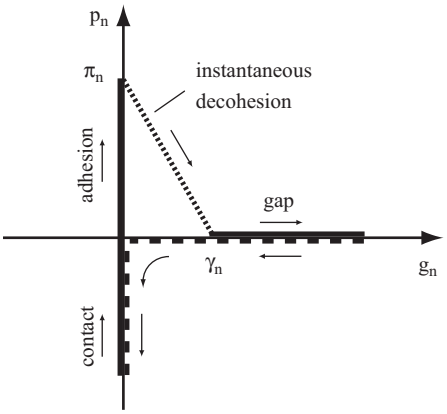

Fig. 2. Graph of a simple normal contact-adhesion law.

3. Specimen design

In an early attempt to estimate the adhesion peak stress π_n between glass and epoxy, simple flat dumbbell (“dog bone”) shaped specimens made of epoxy with an intermediate glass plate in the middle were fabricated (Fig. 3) (deliberately ignoring stress concentrations along interface edges and corners) [8].

The specimens were then pulled on a traction machine. The peak stress π_n could only be coarsely estimated and, even with displacement control, the rupture gap γ_n could never be captured, due to sensitivity of crack initiation to minute interface defects and instability of its subsequent propagation, respectively. In an attempt to stabilize it, the specimen was sandwiched between two elastic rods, without success. It became clear that stable debonding experiments had to be conceived.

3.1. Axisymmetric epoxy-valve on glass-disc specimen

At this stage, it was intuitively conjectured [25] that an axisymmetrical epoxy “trumpet” or “valve” bonded on a glass-disc specimen (Fig. 4) could lead to a stable decohesion, arguing that the crack area would grow with the square of its radius a^2 with such a geometry (instead of its length a in a plane strain geometry). This conjecture found an unexpected support in the simulation of the JKR/Maugis axisymmetrical punch experiments [8] used for illustrating an earlier contact-adhesion law [8,10]. The results showed that the various *convex* punches (flat, conical, parabolic) are the seat of an unstable decohesion process in agreement with the JKR theory but that *concave* punches (in fact concave conical) exhibit a *stable* decohesion process. This is so because the crack nucleates in the centre and its area grows with a^2. The analogy with the valve shape design became clear and reinforced our

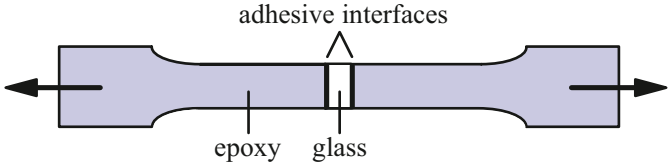

Fig. 3. Epoxy-dumbbell with intermediate glass-plate specimen.

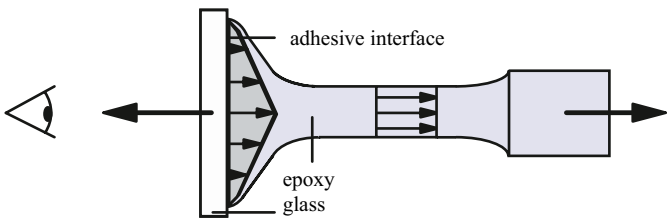

Fig. 4. Axisymmetrical epoxy-valve on glass-disc specimen.

conviction of its validity. A prototypical *axisymmetrical epoxy-valve on glass-disc traction specimen* was designed (Fig. 4).

Before starting the valve-disc specimen fabrication, it was decided to optimize the shape of the epoxy-valve part for uniformizing debonding stability, by means of numerical simulations. To this end the Talon–Curnier contact-adhesion law [10] was used. According to that law, *debonding is stable if the tension stress at the crack front decreases as the crack propagates*, i.e. if the *envelope* of the tension stress at the crack front decreases along the radial axis. The simulations were carried out with the contact analysis program TACT [26].

This was a wise decision because the simulations showed that debonding was nearly stable but still unstable with the conical valve shape shown in Fig. 4. By trial and error, it was found out that a *flat axisymmetric valve was almost stable but yet unstable* (Fig. 5a). Again, using axisymmetric crack geometry comes from the observation that the crack front perimeter $2\pi a$ increases with the radius a as the crack advances from the centre to the periphery with such a geometry (instead of remaining constant in plane strain). From the envelopes plotted in Fig. 5a, it is clear that the axisymmetric geometry (full line) considerably improves the stability of the debonding process in comparison to the plane-strain one (dashed line); but yet not enough. Another stabilizing effect had to be found.

3.2. Concave epoxy-beam on glass-plate specimen

The *plane strain concave epoxy-beam on glass-plate specimen* [27] is inspired from the tapered double cantilever beam (TDCB) used in experimental Fracture Mechanics [28]. This specimen is sketched in Fig. 6 where f is the applied traction, h the half height of the TDCB from its axis and a the crack length measured from the left end of the beam.

For this plane strain beam with a concave increasing "parabolic" profile ($h = h(a)$, $h'(a) > 0$, $h''(a) < 0$), the traction experiment is neutrally stable if the traction force f is a constant function of the displacement u of its point of application [29]. Alternatively, the crack propagation is stable if the crack propagation speed is constant when the opening speed $\dot{u}$ is constant. For the TDCB specimen, the stress intensity factor is

$$K_{\mathrm{I}} = 2\frac{f}{t}m^{1/2}, \quad m = \frac{3a^2}{h^3} + \frac{1}{h}, \tag{5}$$

where t is the beam thickness and m a geometrical parameter relating the beam-height h to the crack-length a (with dimension of an inverse length). The concave "parabolic" profile of the TDCB specimen is defined by requiring $m = \text{const}$, in order to obtain a neutrally stable crack propagation. Hence, a family of homothetical beam

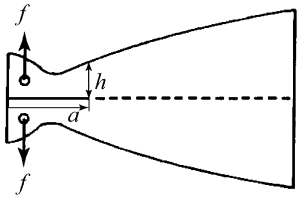

Fig. 6. Tapered double cantilever beam.

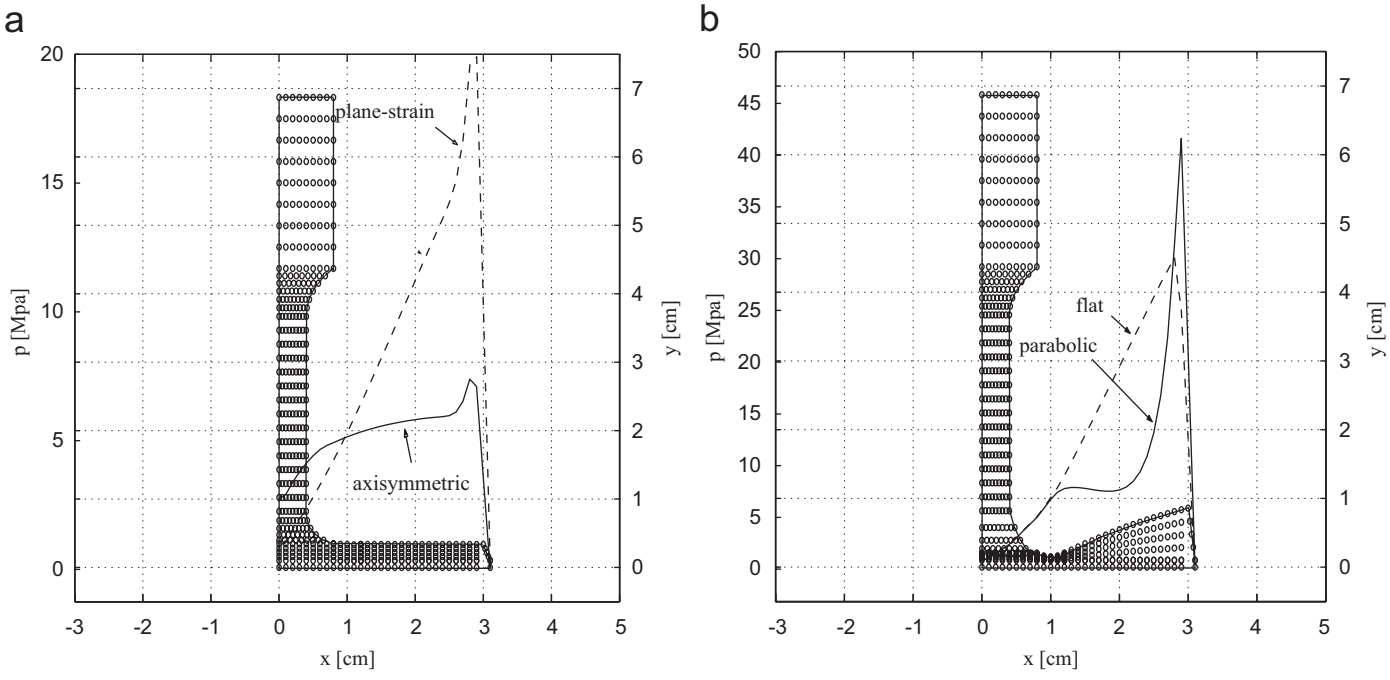

Fig. 5. Envelopes of tension stress at crack front superposed on stamp meshes illustrating the gain in stability brought by (a) axisymmetry and (b) concavity. (a) Axisymmetry vs. plane strain for flat profile; (b) concave vs. flat profile for plane strain beam.

profiles is implicitly defined by

$$mh^3 - h^2 - 3a^2 = 0 \quad (m > 0). \tag{6}$$

The constant m controls the mean height $\bar{h}$ of the beam ($\bar{h}$ decreases as m increases). It can be adjusted by requiring that the maximum stress in the beam remains elastic.

For our adhesion study purpose, the TDCB specimen was modified and adapted into the plane strain concave epoxy-beam on glass-plate specimen shown in Fig. 5(b). The stability of the debonding process was checked by means of a simulation. The envelope of the tension stress at crack front is plotted over the mesh (full line) in Fig. 5b. This envelope confirms that the debonding process is *stable* over a large zone (decreasing part of the curve). The drastic gain in stability brought by the concave increasing "parabolic" profile in comparison to the flat one in plane strain geometry is illustrated by the difference in slope between the two envelope curves (full for parabolic and dashed for flat).

3.3. Axisymmetric concave epoxy-stamp on glass-disc specimen

Combining axisymmetry with a concave (*radial*) *profile does provide a stable debonding process*. Several simulations were run to optimize the concave shape of the epoxy part. The first objective was to uniformize the radial debonding stability and the second one to avoid stress concentrations and plastification of the epoxy.

The final design of the *axisymmetric concave epoxy-stamp on glass-disc specimen* is shown in cross-section in Fig. 7a and in perspective in Fig. 7b. The graph of the tension stress envelope at crack front superposed on the mesh in Fig. 7a shows that the debonding process is *stable* over a large radial zone. Note that the increase and concavity of the stamp is mild in comparison to those of the plane strain beam case (Fig. 5b), due to the underlying axisymmetrical effect.

4. Specimen fabrication

4.1. Mold

The mold for producing an epoxy-stamp on glass-disc specimen is presented in Fig. 8 (closed and open). It is made of aluminum for cooling the epoxy during its polymerization. It is composed of a base ring which holds the glass disc and an axisymmetrical shell in which the stamp is carved and which can be opened into two halves for demolding. The glass disc is pressed between the ring and the shell basis with two intermediate teflon seals to protect the glass and adjust the stamp thickness (height). A series of holes are drilled in the shell, above the upper part of the stamp, to let the air out during epoxy pouring. The mold is filled by pouring the liquid epoxy from the top.

4.2. Glass disc

It is made of mechanical glass (with approximate composition: silicon oxide (silica) SiO_2 60%, aluminum oxide (alumina) Al_2O_3 25%, calcium oxide (lime) CaO 7%, magnesium oxide MgO 6% and boron oxide B_2O_3 2%).

The approximate inertial, elastic and rupture properties of such a brittle glass are

- Density: $\varrho = 2550 \pm 10\,\mathrm{kg/m^3}$.
- Elastic modulus: $\varepsilon = 86.0 \pm 3.0\,\mathrm{GPa}$ (both in tension and compression).
- Ultimate tensile stress: $\chi = 1800 \pm 80\,\mathrm{MPa}$ at $\xi = 0.021 \pm 0.002$ ultimate strain.

The adhesive face of the glass disc is treated with silane to achieve strong bonding with epoxy later on. Roughly speaking, the goal is to arrive at an epoxy–glass adhesion slightly smaller than the epoxy cohesion. To this end, the silane solution used to prepare the disc surface is based on

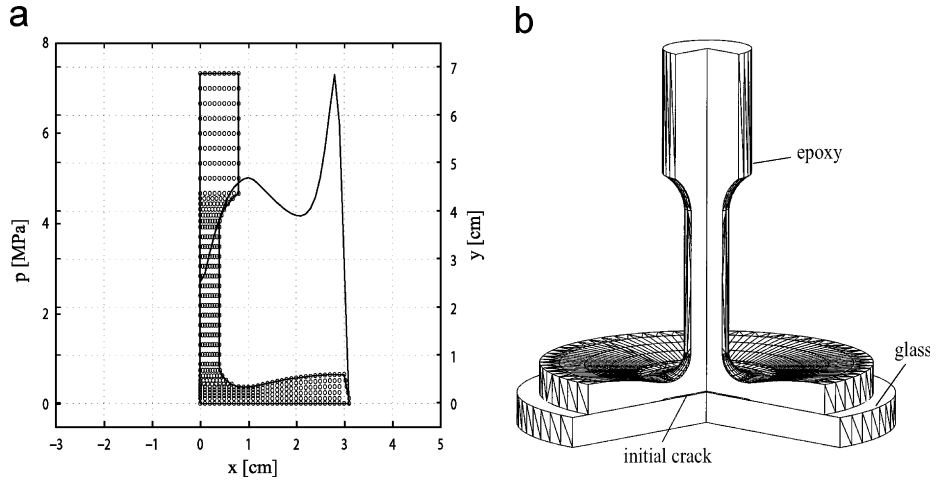

Fig. 7. Axisymmetric concave epoxy-stamp on glass-disc specimen: (a) cross-section with tension envelope and (b) perspective with cut sector.

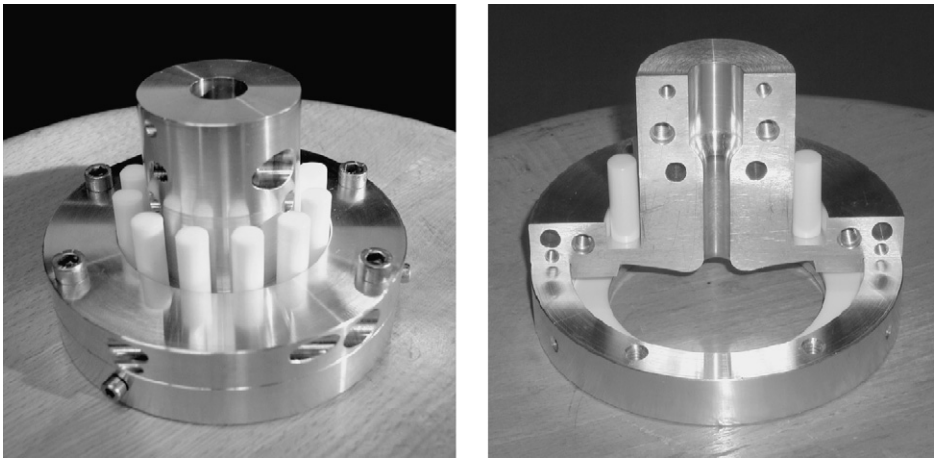

Fig. 8. Mold for production of epoxy-stamp on glass-disc specimen.

the following tentative concentrations:

- 96% pure ethanol,
- 4% distilled water,
- 1.7% silane A-1100.

After being treated with silane, the glass disc is dried either for 2 h in an oven at temperature $T = 100\,^{\circ}\mathrm{C}$ or for 24 h in a desiccator at room temperature $T \approx 25\,^{\circ}\mathrm{C}$.

For initiating the crack after the critical stability radius r, a thin circular film of radius r made of mold release is painted on the glass disc.

4.3. Epoxy-stamp

The epoxy solution used to mold the stamp is based on the following concentrations:

- 70% DER 330,
- 30% DER 732,
- 13% DEH 26.

To prepare the epoxy solution, DER 330 is first heated up to $T \approx 60\,^{\circ}\mathrm{C}$ for 15 min and mixed with DER 732 at the same temperature for 5 min until both components are well liquefied. The hardener DEH 26 is then added to the compound and mixed for 5 min. Finally, the epoxy solution is kept for 5 min in a vacuum chamber, to extract its bubbles.

Traction experiments were carried out on classical dumbbell cylindrical specimens made out of this epoxy, in order to determine its elastic, plastic and rupture properties. The following values were obtained:

- Elastic modulus: $\varepsilon = 2.2 \pm 0.2\,\mathrm{GPa}$ (both in tension and compression).
- Elastic limit stress: $\sigma = 18.0 \pm 2.0\,\mathrm{MPa}$ at $\delta = 0.008 \pm 0.002$ elastic limit strain.
- Ultimate stress: $\chi = 48.6 \pm 0.5\,\mathrm{MPa}$ at $\xi = 0.07 \pm 0.01$ ultimate strain.

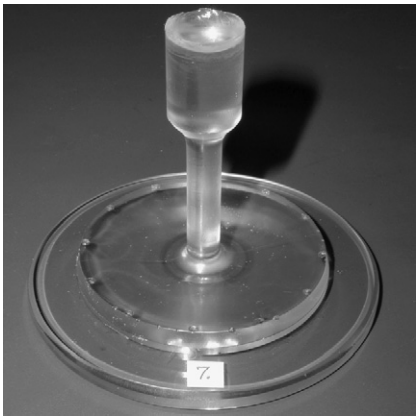

Fig. 9. Axisymmetrical concave epoxy-stamp on glass-disc specimen.

4.4. Molding

To mold the epoxy-stamp on the glass disc, the epoxy solution is poured in the mold and the specimen is left for 24 h at room temperature in its mold. After demolding, the specimen is put in an oven at $T \approx 60\,^{\circ}\mathrm{C}$ for 10 h to complete the polymerization and shorten the curing time.

A picture of a real epoxy-stamp on glass-disc specimen fabricated according to this procedure is shown in Fig. 9.

5. Experimental procedure

An epoxy-stamp on glass-disc specimen is mounted on a standard traction machine (Instron 5800). The complete experimental set-up is sketched in Fig. 10.

The specimen is then pulled or rather elongated. A controlled displacement w is imposed at the rate $\dot{w} = 1\,\mathrm{mm/min}$. The traction force f is measured with the piezoelectric force sensor of the traction machine. The specimen elongation u is measured with an additional linear variable displacement transducer (LVDT) mounted in parallel. Another additional extensometer is mounted on the central cylindrical part of the epoxy-stamp for

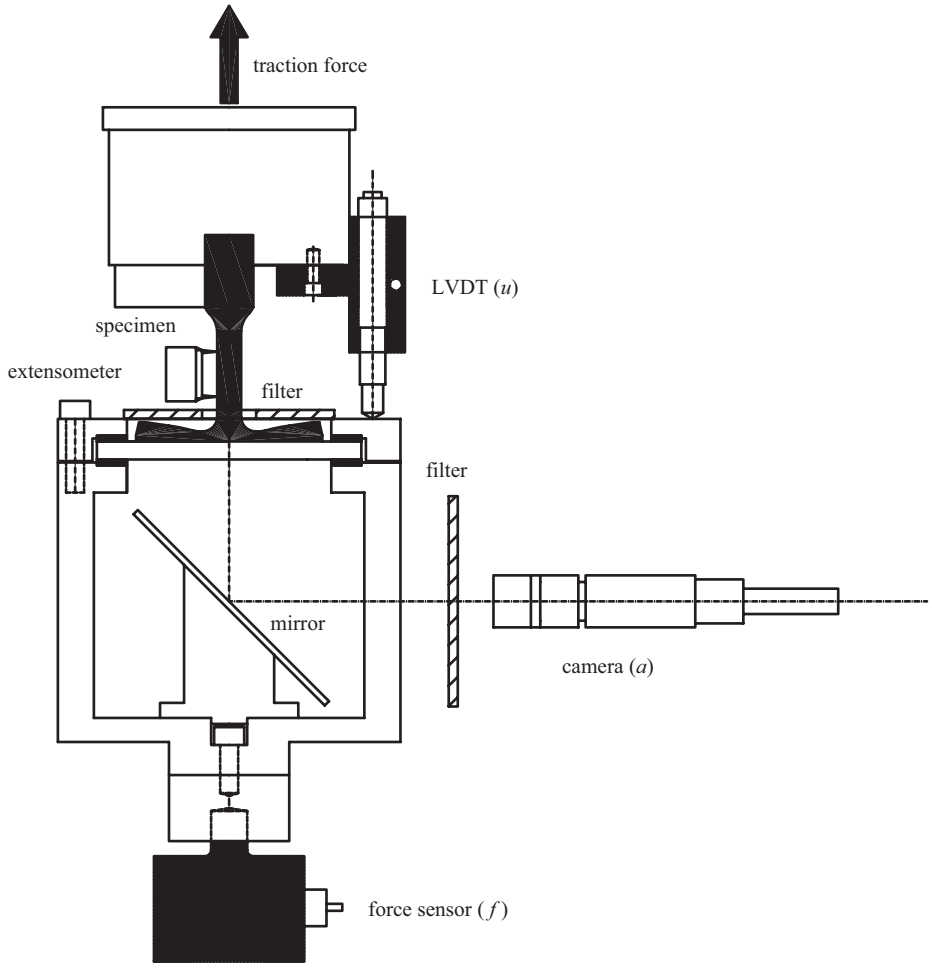

Fig. 10. Diagram of traction experimental set-up (stamp on disc specimen with force and elongation sensors).

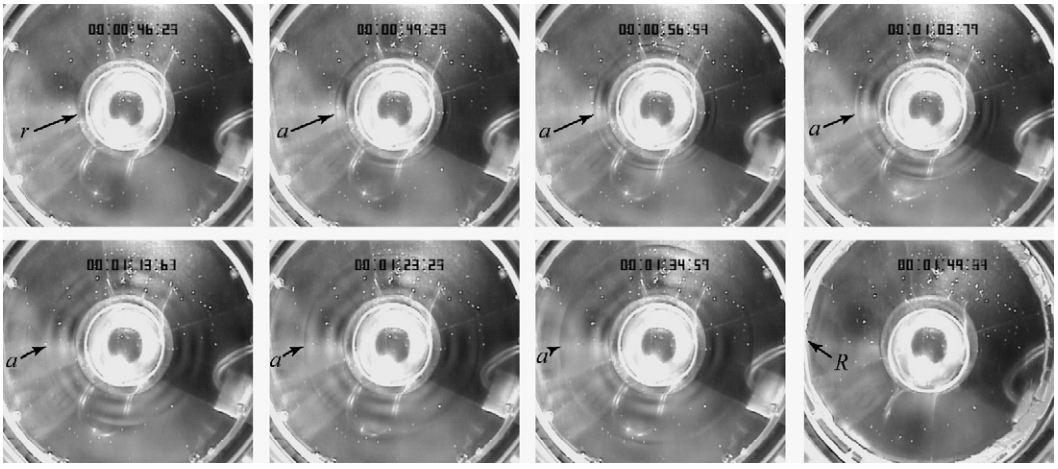

Fig. 11. Crack propagation sequence from the initial internal radius r to the final external radius R passing through "current" crack radii a.

measuring its elongation e and controlling the elastic modulus of the epoxy. A video-camera is installed behind the glass disc for recording the debonding process and measuring the crack radius a. Two optical grade glass polarizing filters are installed for better visualization.

6. Preliminary results

Fig. 11 displays a sequence of photographs recorded by the video-camera through the glass disc and showing the crack propagation. The crack starts at its initial radius r

and expands radially in a stable way as the load is increased, up to a critical radius R where it becomes unstable and deviates in the epoxy-stamp (which breaks along a cylindrical surface). Axisymmetry, in particular circularity of the crack front, is perfectly conserved throughout the debonding process.

The force histograph $f = f(t)$ is shown in Fig. 12a. The crack initiation (point A at radius r) and termination (point B at R) are easy to identify on this graph. It is clear that the debonding process is *stable* between A and B since an increasing force is necessary for advancing the crack from r to R. The early discontinuity (point C) corresponds to the (sudden) debonding of the mold release film interposed for initiating the crack.

A set of force histographs for a few specimens is presented in Fig. 13. There are two pairs of curves: curves 1 and 2 correspond to specimens (the glass disc of which were) dried for 2 h in the oven, whereas curves 3 and 4 correspond to specimens dried for 24 h in the desiccator.

It can be (qualitatively) concluded that short and hot drying in an oven produces stronger adhesion between glass and epoxy than long and cold drying in a desiccator. This well-known influence of humidity on glass–epoxy adhesion was not further (quantitatively) investigated since our main objective was to obtain a stable debonding experiment rather than to study adhesion in itself, in this preliminary phase of our research.

The excellent reproducibility of the results from one experiment to the next (for a given drying mode) must be emphasized.

7. Identification of adhesive properties

The adhesion properties (surface energy ω, peak stress π_n and rupture gap γ_n, out of which only two are independent due to (1)) can be extracted from the experimental measurements (specimen elongation u, traction force f and crack radius a) by the following procedure.

According to our simple adhesion–decohesion law, the adhesion surface energy or decohesion dissipation per unit area is [cf. (1)]

$$\omega = \tfrac{1}{2}\pi_n\gamma_n. \tag{7}$$

The work dissipated between the initial crack radius r and the current one a is equal to the dissipation per unit area multiplied by the debonded area $A = \pi(a^2 - r^2)$:

$$\Omega = \omega A = \tfrac{1}{2}\pi_n\gamma_n\pi(a^2 - r^2). \tag{8}$$

Firstly, this dissipated energy Ω is measured on the experimental force–displacement graph $f = f(u)$ (Fig. 14). It is equal to the area of the hysteresis loop obtained upon elastic unloading. Elastic unloading can be either idealized as linear or measured from a real experimental unloading (experimental unloading is more accurate because it takes into account the elastic nonlinearity of epoxy and allows to detect its plastic deformation if any).

Secondly, the measured traction force f or prescribed specimen elongation u at the initial crack radius r is used as a boundary condition in a simulation of the stamp (free between 0 and r and fixed between r and R at its basis), with the contact analysis program TACT, in order to evaluate the adhesion peak stress π_n.

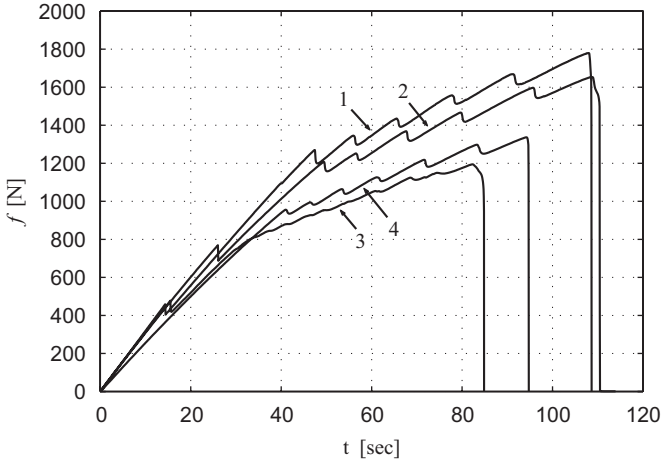

Fig. 13. Force histographs for differently dried silane coated glass discs.

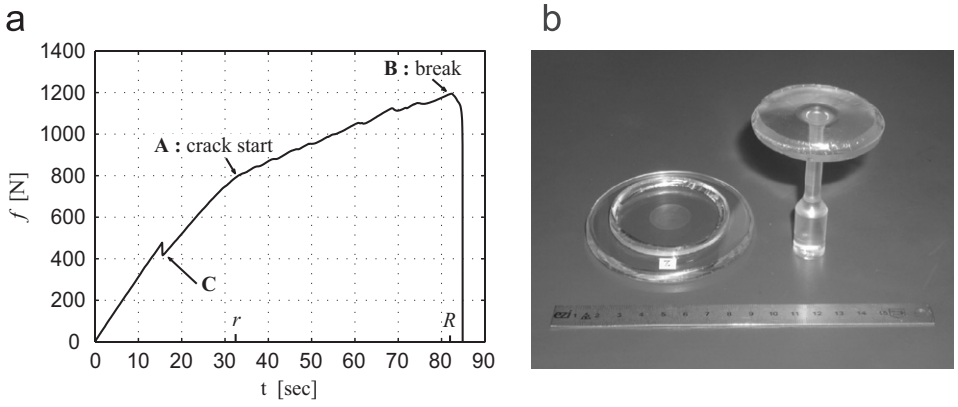

Fig. 12. Force histograph and broken stamp-disc specimen: (a) force histograph and (b) glass disc and epoxy-stamp after rupture.

Finally, the (dependent) rupture gap γ_n is calculated by solving Eq. (8) for it

$$\gamma_n = 2\frac{\omega}{\pi_n} = 2\frac{\Omega}{\pi(a^2 - r^2)}\frac{1}{\pi_n}. \quad (9)$$

The following *preliminary estimates* of the adhesive properties between glass and epoxy were found, using the above identification procedure (Table 1).

Finally, Fig. 15 presents a comparison of an experimental traction–elongation graph and a numerical simulation one obtained with TACT. The numerical simulation was run with the adhesion peak stress $\pi_n = 17.4$ MPa ($=$ const) as criterion for crack propagation (and the decohesion rupture gap $\gamma_n = 21.8\,\mu$m, inactive in a monotonous loading experiment). Hence, when the tensile stress at crack front reaches this value, the crack starts and propagates in stable way until the final critical radius R. We can see that the numerical solution is in good agreement with the experimental response. The early discontinuity, corresponding to the debonding of the mold release film interposed for initiating the crack, is accounted for in the simulation.

8. Conclusion

The *epoxy-stamp on glass-disc specimen* is believed to be a major advance in experimental adhesion mechanics since it is the seat of *stable debonding*. Debonding stability is achieved by combining axisymmetry with concavity of the epoxy-stamp. It is confirmed by the actual experiments. It allows for an accurate identification of the adhesive properties ω, π_n and γ_n between glass and epoxy. Actual elastic unloading is expected to improve further the accuracy.

The epoxy-stamp on glass-disc specimen can of course be used to study the adhesion and decohesion between glass and epoxy. It was already found that the drying mode of the glass disc after its treatment with silane has an influence on them. The influence of other parameters such as the compositions of the glass and the epoxy, the curing time of the epoxy, the test temperature, ... can obviously be studied.

The good agreement between numerical and experimental results confirm the validity of our simple adhesion–decohesion law with tension threshold π_n and an instantaneous brittle decohesion over a finite gap γ_n. The same experiment can probably be used to study more sophisticated laws with viscous or plastic decohesion for instance.

The stamp on disc specimen design can be used for other pairs of materials (provided one can be molded on the other). Finally, it can perhaps be adapted into a torsion experiment to study adherence and decoherence. Combining torsion with compression on a torsion–traction machine may permit to find out whether adherence depends on pressure or not.

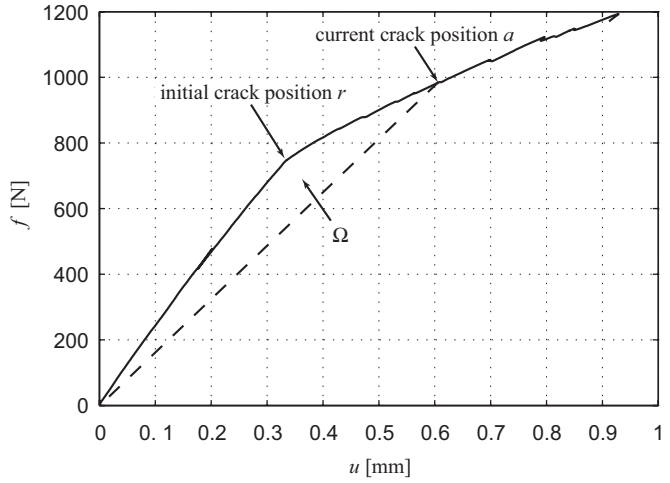

Fig. 14. Force-displacement curve.

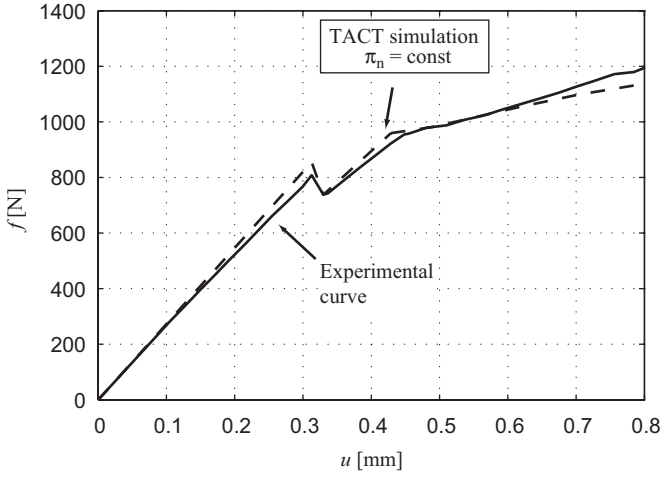

Fig. 15. Comparison of numerical simulation with experimental results.

Table 1
Preliminary results

Glass drying mode after silane treatment	r (mm)	a (mm)	A (mm^2)	Ω (N/mm)	ω (N/mm)	π_n (MPa)	γ_n (μm)
2 h in oven at $T = 100\,^\circ$C	11.4	15.5	349.0	118.0	0.34	23.0	29.4
24 h in desiccator at $T \approx 25\,^\circ$C				66.4	0.19	17.4	21.8

Acknowledgement

The authors gratefully acknowledge the financial support of Swiss National Science Foundation, project 2000-066758, which made this work possible.

References

[1] Atkins AG, Mai YW. Elastic and plastic fracture, Chichester, UK: Ellis Horwood; 1985/1988.
[2] Burridge R, Keller JB, Peeling. slipping and cracking—some one-dimensional free-boundary problems in mechanics. SIAM Rev 1978;20(1):31–61.
[3] Barquins M. Sur le pelage spontané des élastomères. C R Acad Sci Paris Ser II 1984;298:725–30.
[4] Johnson KL, Kendall K, Roberts AD. Surface energy and the contact of elastic solids. Proc R Soc London Ser A 1971;324:301–13.
[5] Savkoor A. Dry adhesive friction of elastomers. PhD thesis, Technical University of Delft; 1987.
[6] Maugis D, et al. The JKR–DMT transition in the presence of a liquid meniscus and the extension of the JKR theory to large contact radii, In: Raous M, editor, Contact mechanics. New York: Plenum Press; 1994.
[7] Maugis D. Contact, adhesion and rupture of elastic solids. Heidelberg: Springer; 2000.
[8] Talon C., Couplage d'une loi d'adhésion à une loi de contact avec frottement pour l'étude de la décohésion dans les matériaux composites. PhD thesis, Ecole Polytechnique Fédérale de Lausanne 2001.
[9] Curnier A, He Q-C, Klarbring A. Continuum mechanics modelling of large deformation contact with friction. In: Raous M, et al., editors. Contact mechanics. New York: Plenum; 1995. p. 145–58.
[10] Talon C, Curnier A. A model of adhesion coupled to contact and friction. Euro J Mech A/Solids 2003;22:545–65.
[11] Mozynski W. Frottement des corps solides dans les cas de l'anisotropie naturelle et artificielle, Bull Int Acad Pol Sci Lett Cl Sci Math Nat Sér A: Sci Math Cracov (Supp. 4): 1951; 447–86.
[12] Moreau JJ. Sur les lois de frottement, de plasticité et de viscosité. C R Acad Sci Paris Ser A 1970;271:608–11.
[13] Fredriksson B. Finite element solution of surface nonlinearities in structural mechanics with special emphasis to contact and fracture mechanics problems. Comput Struct 1976;6:281–90.
[14] Michalowski R, Mroz Z. Associated and non-associated sliding rules in contact friction problems. Arch Mech 1978;30(3):259–76.
[15] Curnier A. A theory of friction. Int J Solids Struct 1984;20(7):637–47.
[16] Klarbring A. General contact boundary conditions and the analysis of frictional systems. Int J Solids Struct 1986;22(12):1377–98.
[17] Curnier A, Alart P. A generalized Newton method for contact problems with friction. J Mécan Théor Appl 1988; 7(1):67–82 [special issue "Numerical methods in mechanics of contact involving friction." Raous M, editor].
[18] Frémond M. Adhérence des solides. C R Acad Sci Paris Ser II 1982;295:769–72.
[19] Frémond M. Contact unilatéral avec adhérence. In: Del Piero GP, Maceri F, editors. Unilateral problems in structural analysis. Heidelberg: Springer; 1985.
[20] Frémond M. Contact unilatéral avec adhérence. In: Del Piero GP GP, Maceri F, editors. Unilateral Problems in Structural Analysis. Heidelberg: Springer; 1987.
[21] Truong DT. Contact avec adhérence. PhD thesis, University of Paris VI; 1990.
[22] Cangémi L, Cocu M, Raous M. Adhesion and friction model for the fiber–matrix interface of a composite, In: Proceedings of the ASME-ESDA-96 Symposium Montpellier; 1996.
[23] Raous M, Cangémi L, Cocu M. A consistent model coupling adhesion, friction and unilateral contact. Comput Methods Appl Mech Eng 1999;177:383–99.
[24] Curnier A, Talon C. Unilateral contact and dry friction with adhesion, a source of instability. In: Colloque Instabilité du frottement, Chambéry; 1999.
[25] Curnier A. Trumpet specimen to study adhesion. LMAF archives, 2000.
[26] Curnier A. Computational methods in solid mechanics. Dordrecht: Kluwer Academic Publishers; 1994.
[27] Sekulic A. TDCB model to study adhesion. LMAF archives, 2004.
[28] Kinloch AJ, Young RJ. Fracture behaviour of polymers. Barking: Applied Science Publishers; 1983.
[29] Gurney C, Mai YW. Stability of cracking. Eng Fract Mech 1972;4:853–63.